

See discussions, stats, and author profiles for this publication at: <https://www.researchgate.net/publication/268232187>

Molecular Adhesion at Clay Nanocomposite Interfaces Depends on Counterion Hydration—Molecular Dynamics Simulation of Montmorillonite/Xyloglucan

ARTICLE *in* BIOMACROMOLECULES · NOVEMBER 2014

Impact Factor: 5.75 · DOI: 10.1021/bm5014525 · Source: PubMed

CITATION

1

READS

49

7 AUTHORS, INCLUDING:



Jakob Wohlert

KTH Royal Institute of Technology

26 PUBLICATIONS 541 CITATIONS

[SEE PROFILE](#)



Malin Bergenstråhle-Wohlert

KTH Royal Institute of Technology

23 PUBLICATIONS 439 CITATIONS

[SEE PROFILE](#)



Yaoquan Tu

KTH Royal Institute of Technology

69 PUBLICATIONS 631 CITATIONS

[SEE PROFILE](#)



Hans Agren

KTH Royal Institute of Technology

866 PUBLICATIONS 18,699 CITATIONS

[SEE PROFILE](#)

Molecular Adhesion at Clay Nanocomposite Interfaces Depends on Counterion Hydration—Molecular Dynamics Simulation of Montmorillonite/Xyloglucan

Yan Wang,[†] Jakob Wohlert,^{*,‡,§} Malin Bergenstråhle-Wohlert,^{‡,§} Joby J. Kochumalayil,^{‡,§} Lars A. Berglund,^{‡,§} Yaoquan Tu,[†] and Hans Ågren^{*,†}

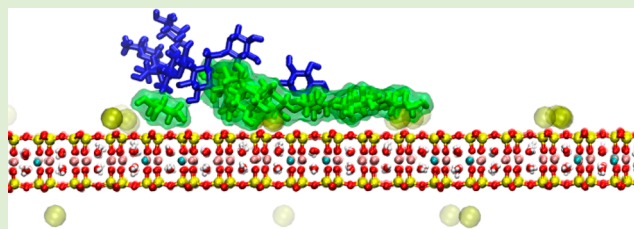
[†]Division of Theoretical Chemistry and Biology, School of Biotechnology, KTH Royal Institute of Technology, SE-106 91 Stockholm, Sweden

[‡]Department of Fibre and Polymer Technology, School of Chemical Science and Engineering, KTH Royal Institute of Technology, SE-100 44 Stockholm, Sweden

[§]Wallenberg Wood Science Centre, KTH Royal Institute of Technology, SE-100 44 Stockholm, Sweden

Supporting Information

ABSTRACT: Nacre-mimetic clay/polymer nanocomposites with clay platelet orientation parallel to the film surface show interesting gas barrier and mechanical properties. In moist conditions, interfacial adhesion is lowered and mechanical properties are reduced. Molecular dynamic simulations (MD) have been performed to investigate the effects of counterions on molecular adhesion at montmorillonite clay (Mnt)—xyloglucan (XG) interfaces. We focus on the role of monovalent cations K^+ , Na^+ , and Li^+ and the divalent cation Ca^{2+} for mediating and stabilizing the Mnt/XG complex formation. The conformation of adsorbed XG is strongly influenced by the choice of counterion and so is the simulated work of adhesion. Free energy profiles that are used to estimate molecular adhesion show stronger interaction between XG and clay in the monovalent cation system than in divalent cation system, following a decreasing order of K-Mnt, Na-Mnt, Li-Mnt, and Ca-Mnt. The Mnt clay hydrates differently in the presence of different counterions, leading to a chemical potential of water that is highest in the case of K-Mnt, followed by Na-Mnt and Li-Mnt, and lowest in the case of Ca-Mnt. This means that water is most easily displaced from the interface in the case of K-Mnt, which contributes to the relatively high work of adhesion. In all systems, the penalty of replacing polymer with water at the interface gives a positive contribution to the work of adhesion of between 19 and 35%. Our work confirms the important role of counterions in mediating the adsorption of biopolymer XG to Mnt clays and predicts potassium or sodium as the best choice of counterions for a Mnt-based biocomposite design.



INTRODUCTION

Nature is an excellent source of inspiration for the development of new functional materials. Bioinspired or biobased gas barrier films have included biopolymers¹ and hemicelluloses,² but also polylactides with bioinspired morphologies.³ The classical “brick-and-mortar” arrangement, which plays a key role for the outstanding mechanical properties of nacre,⁴ has inspired the development of a new class of green materials to replace conventional petroleum-based plastic films. These artificial nacre-like materials^{5,6} are nanocomposites based on the biopolymer xyloglucan (XG) and montmorillonite clay (Mnt). In order to optimize the mechanical properties of these materials, the load transfer between the soft polymer and the stiffer clay platelets as well as the dispersion of the clay platelets within the matrix is crucial. Both load transfer and dispersibility strongly depend on the wet adhesion between the polymer matrix and the clay platelets, and it is a considerable challenge to obtain a well dispersed clay mineral in the polymer matrix to mimic the material architecture of nacre.⁵

As computer models become increasingly more realistic, atomistic molecular dynamics computer simulation has during the past decades evolved into a tool suitable for addressing specific questions in materials science in general, and clay minerals and polymer–clay interactions in particular.^{7,8} We have recently used large-scale atomistic MD simulations to study the adhesion of XG to Na-Mnt in the wet state.⁹ It was found that strong electrostatic interactions between XG and clay, in combination with low conformational freedom of the XG molecule due to its relatively stiff backbone leads to a considerable work of adhesion also at full hydration. This could explain the extraordinary mechanical properties of XG/Na-Mnt composites, even at high relative humidity (RH). The present study takes as a starting point the unexpected experimental observation that when sodium is replaced by

Received: September 30, 2014

Revised: November 10, 2014

Published: November 12, 2014

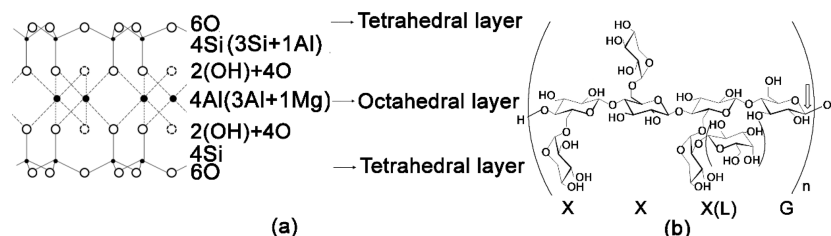


Figure 1. Structures of (a) the Mnt clay unit cell, and (b) the basic oligosaccharide repeat unit.

potassium or calcium through ion exchange, the tensile properties at high RH of the final composite is significantly affected. This observation motivates a detailed study of the role of counterions for the adhesion within these systems.

It has previously been reported that the choice of counterions plays an important role in the swelling of Mnt clay in the hydrated state,^{10–13} and it was noted that this effect strongly correlates with the hydration of the respective cation. Furthermore, Coveney and co-workers have used molecular simulations to study how the swelling of clays is inhibited by the adsorption of different organic polymers to the clay^{14,15} and they conclude that the amount of organic material that can be adsorbed also correlates with the hydration of the cations. Specifically, they find that adhesion of polyalkylene glycols and polyalkylene oxides are enhanced in the case of K-Mnt compared to Na-Mnt and Li-Mnt, which they attribute to that the weaker hydration of K⁺ compared to Na⁺ and Li⁺ makes water molecules more easily displaced from the clay/polymer interface. Interestingly, they also conclude that molecules with good adhesion to Mnt clay ideally should be long oligomers with both hydrophilic and hydrophobic moieties,¹⁴ which is a description that fits XG very well.

We have used extensive MD simulations of an XG fragment interacting with a model Mnt clay surface at full hydration, in the presence of K⁺, Na⁺, Li⁺, or Ca²⁺ as counterions. The work of adhesion between XG and clay was estimated from steered MD simulations, by slowly pulling the XG off the clay surface. To elucidate the mechanisms by which the choice of counterions affects molecular adhesion, the XG/clay interface was characterized by radial distribution functions (RDFs) and one-dimensional density plots. Finally, the proposed mechanism that differences in adhesion depend on ease of water expulsion from the interface is investigated by a calculation of the chemical potential of interfacial water in the presence of different cations.

METHODS

Theoretical Model. Following our previous study⁹ of XG adsorption on Mnt clay, we built a simplified model for XG by linking two oligosaccharide units, XXLG and XXXG (see Figure 1), with an additional glucose unit attached to the reducing end, resulting in the sequence (GXXLGXXXG). This corresponds to a molecular weight of 2.9 kDa, which is certainly much lower than native XG, but high enough to show a clear affinity for Mnt clay surfaces.⁹ The clay sheet was built by replicating the structure M_{0.75}[Si_{7.75}Al_{0.25}](Al_{3.5}Mg_{0.5})O₂₀(OH)₄ in the lateral directions, giving a rectangular slab of approximately 8.3 by 9.0 nm. Here M represents the counterions, which are either of K⁺, Na⁺, Li⁺, or Ca²⁺.

The clay and the XG were put in a periodical orthorhombic box with the same lateral dimensions as the clay sheet, making the sheet effectively infinite in size, and a height of 8 nm. A number of counterions were distributed randomly across the simulation box (60 in the case of Ca²⁺, 120 in the case of the monovalent ions), and finally, the box was solvated using approximately 17000 water molecules, resulting in a system comprised of more than 58000 atoms. The appearance of the

molecular model is shown in Figure 2. The initial configurations were relaxed by performing 150 ns of molecular dynamics, during which the XG spontaneously adsorbed to the Mnt surface.

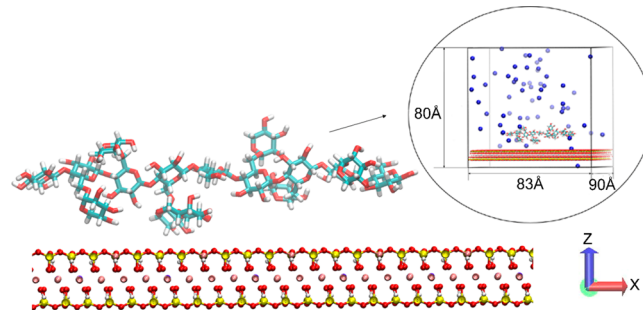


Figure 2. Molecular graphics representation of the XG-Mnt model in its initial configuration, showing the Mnt clay, the XG, counterions, and box dimensions. Water molecules are not shown for clarity.²⁶ Color scheme is as follows: O (red), H (white), C (cyan), Si (yellow), Al (pink), Mg (dark blue), and counterions (light blue).

Force field parameters were taken from CLAYFF¹⁶ for the Mnt clay, GLYCAM06¹⁷ for the XG, and water was described by the simple point charge (SPC) model.¹⁸ The nonbonded parameters for the ions were taken from literature.^{19,20}

Computational Details. Molecular dynamics simulations were performed using the GROMACS/4.5.5 simulation package,^{21–25} with a basic time step of 1 fs, and with energies and coordinates stored every 10 ps. Equilibrium properties were calculated from the last 40 ns of the 150 ns trajectories mentioned above. In addition, to assess the molecular adhesion of XG to Mnt, the Potential of Mean Force (PMF) pertaining to the desorption process was calculated by umbrella sampling, with the perpendicular distance between the clay surface and the center of mass of the XG as reaction coordinate. For each system, a total of 120 umbrella windows were used, and each window was simulated for 3 ns, with coordinates and forces stored every 1 ps. A more detailed description of both model and simulation protocol can be found as Supporting Information. Molecular graphics were produced using VMD.²⁶

Tensile Tests. Nanocomposites based on Mnt clay platelets and XG were prepared according to a procedure described elsewhere⁵ using three different counterions (K⁺, Na⁺, and Ca²⁺). The Mnt content in each composition was 50–60 wt %. Tensile testing was performed on an Universal testing machine (Instron 5944) with a load cell of 500 N. The films were cut in rectangular strips of dimension 3 × 20 × 0.03 mm³ and conditioned at 23 °C and 92%RH for at least 24 h. Six specimens were tested from each sample. Statistical significance was evaluated using one-way ANOVA tests.

RESULTS AND DISCUSSION

Mechanical Properties of Nanocomposites. The mechanical properties of the different Mnt/XG nanocomposites were evaluated by tensile tests at high relative humidity and the results are presented in Table 1. Surprisingly, the choice of counterion had an effect on the mechanical performance of the

Table 1. Mechanical Properties from Tensile Tests of Mnt-XG Composites with Different Counterions

sample	elastic modulus (GPa)	tensile strength (MPa)	tensile strain to failure (%)
Na-Mnt/XG	7.3 ± 0.8	42.3 ± 9.6	1.10 ± 0.42
K-Mnt/XG	8.9 ± 0.9	62.1 ± 8.7	1.38 ± 0.44
Ca-Mnt/XG	7.3 ± 0.9	51.8 ± 8.5	1.45 ± 0.35

material, where K-Mnt/XG gave the highest modulus and tensile strength whereas Ca-Mnt/XG and Na-Mnt/XG were significantly lower in both stiffness (statistical *p*-value of 0.008) and strength (*p* = 0.02). An earlier study has shown a strong effect of interfacial adhesion on tensile properties, especially in the presence of moisture.⁵ The results in Table 1 therefore indicate that the counterions play an important role for the Mnt/XG adhesion mechanisms, and this motivates the computational work in the present study.

Molecular Adhesion. Here we investigate molecular adhesion by computational modeling in order to enlighten the effect of different counterions. Mechanical and thermal properties of biopolymer-based composites are strongly dependent on the adhesion of the biopolymer to the reinforcing component.⁴ Furthermore, molecular adhesion also plays an important role during the making of the material as it is closely related to the adsorption of the polymer to the clay surface.

The molecular adhesion can be estimated from the work of adhesion, W_A , of single XG fragments, that is, the reversible work needed to pull the polymer off the clay surface, into the aqueous phase. Here, the free energy profile pertaining to such a desorption process is obtained from MD simulations using umbrella sampling. The results are shown in Figure 3, where W_A

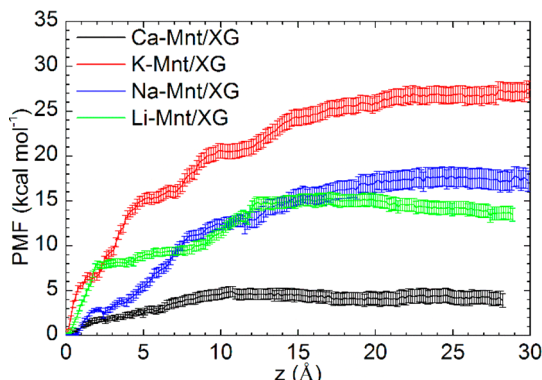


Figure 3. Free energy profiles of the desorption process of XG from Mnt clay surfaces in the presence of different counterions. The *x*-axis refers to the center-of-mass distance between XG and Mnt, parallel to a vector perpendicular to the clay surface. The value is measured relative to the adsorbed conformation in each system (see Figure 4). The *y*-axis denotes the work of adhesion (W_A) in kcal mol⁻¹.

is calculated as the free energy difference between the adsorbed state ($z = 0$) and the value where the curves have leveled off, meaning that the XG is fully detached from the clay. It is found that the largest adhesion between XG and Mnt is found for the K-Mnt system, where $W_A = 26.9 \pm 1.0$ kcal mol⁻¹. Then follows, in decreasing order, Na-Mnt ($W_A = 17.5 \pm 1.1$ kcal mol⁻¹), Li-Mnt ($W_A = 15.3 \pm 0.7$ kcal mol⁻¹), and finally the lowest adhesion is found in the Ca-Mnt system with $W_A = 4.9 \pm 0.6$ kcal mol⁻¹.

Note that the W_A calculated here does not represent the complex macroscopic adhesion phenomena in a real system.

Instead, it is a representation of the molecular adhesion, which is a result of chemical and physical interactions at the microscopic level. In spite of that, calculated values for W_A correlates with the tensile properties obtained for the real composite materials at high relative humidity (Table 1) in the sense that K-Mnt/XG, which exhibits the best adhesion, also gives the best mechanical performance. However, Ca-Mnt/XG, which shows almost negligible adhesion compared to the other systems, actually performs better than Na-Mnt/XG. This shows, not very surprisingly, that microscopic adhesion alone is not sufficient to fully explain the final properties of the composite material. Other factors, such as counterion effects on the colloidal state and dispersion of Mnt platelets, XG physical entanglements, and that the materials are not completely wet, are also important.

Interfacial Structure and Competing Mechanisms. The interfaces in the studied Mnt/XG systems with different ions are complex, and all different components (ions, water, XG, and Mnt) affect the overall properties. To separate the competing mechanisms acting for or against the adhesion between XG and Mnt we consider one or a couple of components at a time.

XG and Ions at the Interface. A computation of the number of contacts between the XG and the Mnt surface (Figure 4, left panel) is helpful to explain the large difference in W_A between the different systems. It represents the total number of sugar residues in close contact (within 4 Å) with the clay surface in equilibrium. For K-Mnt, 15 out of 17 residues are adsorbed, followed by 10 in the case of Na-Mnt, 7 for Li-Mnt, and finally only 4 sugar residues in the case of Ca-Mnt. As presented in Figure 1, the reason is that XG has different adsorbed conformations depending on the counterion. When these numbers are compared to W_A , one finds that each contact gives a fairly constant contribution to W_A , amounting to, approximately, 2 kcal mol⁻¹, regardless of ion species, except in the case of Ca when the corresponding number is approximately 1 kcal mol⁻¹ per contact. Residues further away from the surface will also, of course, also interact with the clay. However, it is a fair approximation that residues in close contact with the clay will dominate the interaction energy since XG/clay interactions are dominated by electrostatics⁹ and, also, considering the high relative permittivity and effective screening of water. However, it is puzzling that a contact is worth less in terms of free energy in Ca-Mnt than in the other systems, and this indicates that this picture might be an oversimplification. Furthermore, it does not explain why the number of contacts varies as it does.

The differences in adsorption among different cations are also manifested in the number of hydrogen bonds between the XG and water. When the XG detaches from the surface, XG/water hydrogen bonding increases, since hydroxyl groups that earlier were interacting with the clay now become hydrated. The increase in number of XG/water hydrogen bonds is largest in the case of K-Mnt, where it amounts to 15 hydrogen bonds, followed by Na-Mnt with 10 bonds, Li-Mnt with 9, and finally, Ca-Mnt, where the increase is less than one hydrogen bond (see Table S2 in Supporting Information). This means that, in the case of Ca-Mnt, hydrogen bonding between XG and the Mnt clay is basically nonexistent.

The structural dynamics of the XG is also affected by how well it adsorbs to the surface. One indicator of the flexibility of the adsorbed XG is the fluctuations of the radius of gyration (see Figure S3 in Supporting Information), which is largest in the case of Ca-Mnt and smallest for K-Mnt. A principal component analysis also reveals that the dynamics of XG is more restricted in the K-Mnt and Na-Mnt systems than for the Li-Mnt and Ca-Mnt

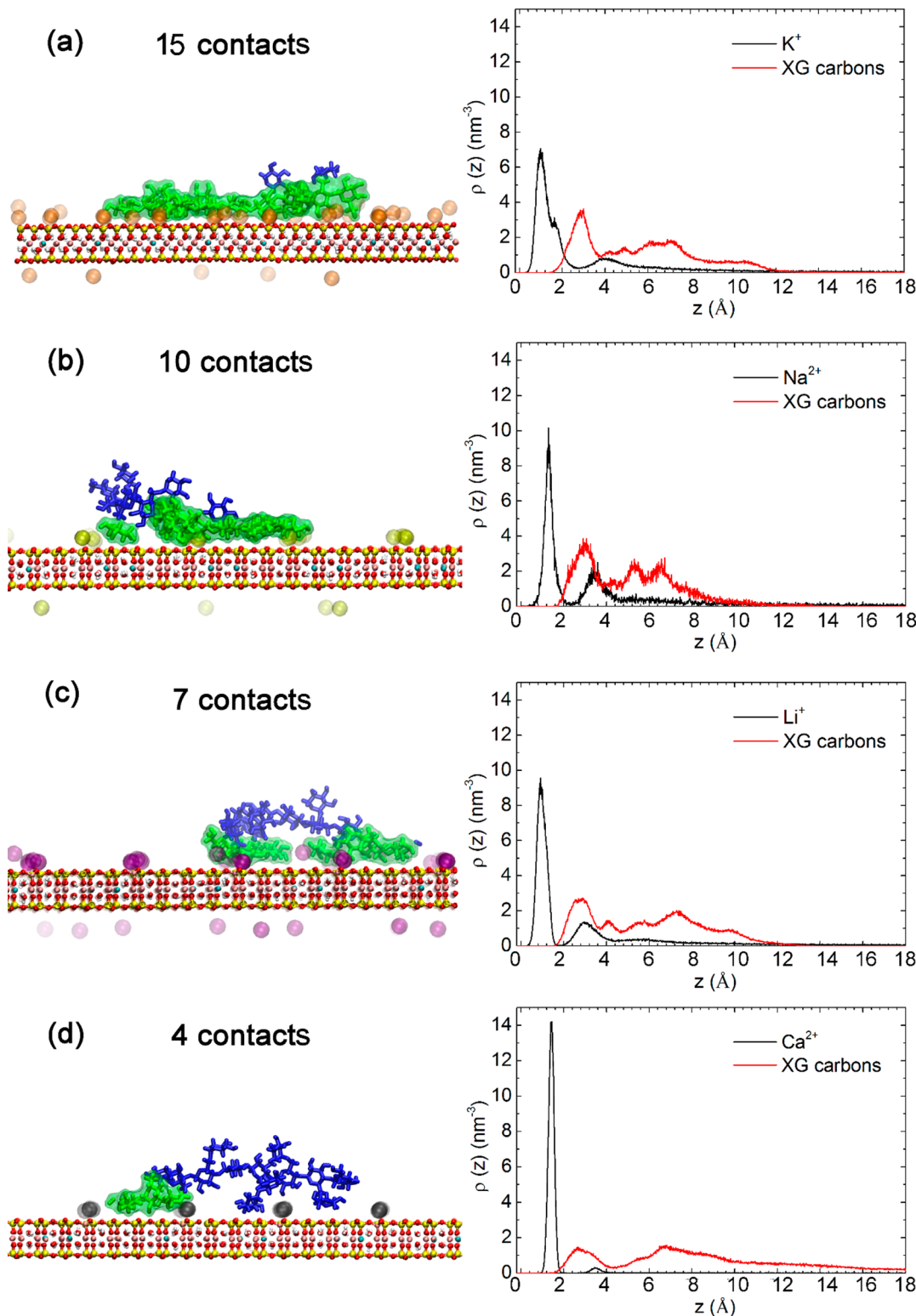


Figure 4. Molecular graphics of XG adsorbed to Mnt in the presence of different counterions (left) and number density $\rho(z)$ of ions and XG carbons as a function of perpendicular distance z from the Mnt surface (right). The number of contacts are the number of residues within 4 Å of clay surface. The color codes in the left panel are residues in contact with clay (green transparent surface); residues detached from clay (blue opaque); K⁺ (orange transparent surface); Na²⁺ (yellow transparent surface); Li⁺ (magenta transparent surface); Ca²⁺ (gray transparent surface).

systems (see Figure S4 in Supporting Information). It also shows quite obviously, that a strongly adsorbed XG molecule in a nanocomposite interphase region behaves very differently compared to one in solution.

The ability of XG to adsorb to Mnt clay can evidently be made dramatically different by changing the ion species present in the system. However, kinetics aspects also need to be considered. Adsorption in these systems is a slow process, and already, for the case of K-Mnt, which gives the best adhesion, it takes place on a

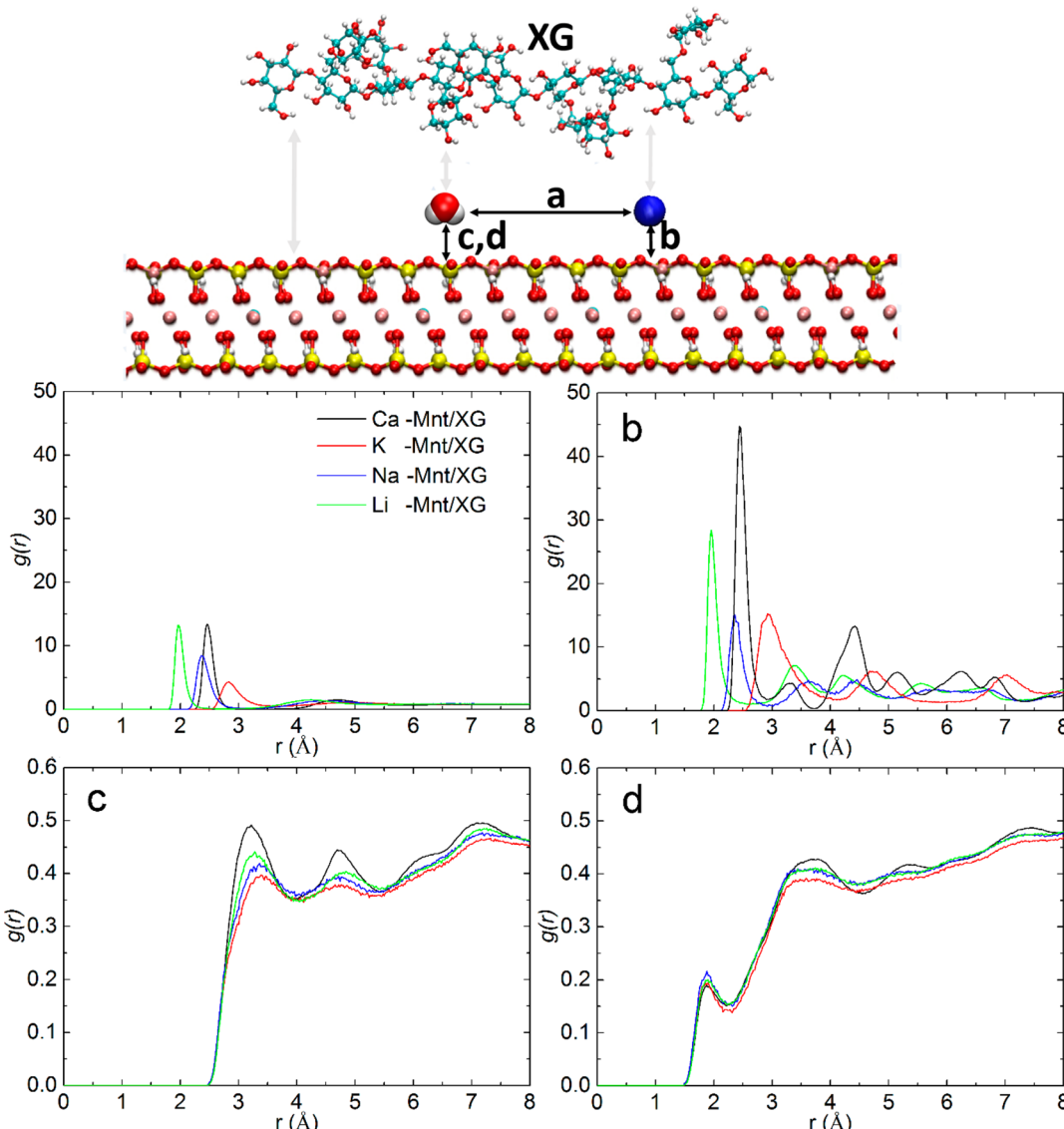


Figure 5. Top: A schematic picture of the interfacial structure, where a–d are indicating between which pairs the radial distribution function (RDF), denoted $g(r)$, was calculated: (a) between counterions and water oxygen; (b) between counterions and clay tetrahedral oxygen; and finally, between clay tetrahedral oxygen and water oxygen (c) or hydrogen (d).

100 ns time scale, which is close to what is feasible using atomistic modeling. This could indicate that there are large energy barriers associated with this process. It is quite possible that changing ion species also affects these barriers, without changing the actual energy levels. In that case, the observed difference between the systems would be a kinetic effect, although still of practical importance. There are indications of such barriers in Figure 3, especially in the curve representing the K-Mnt system, which seems to increase in a stepwise manner. This is an effect of that the sugar residues are pulled off sequentially. However, the fact that the barriers are very small indicates that the simulations really are representing thermodynamic equilibrium and, thus, are useful to assess the molecular adhesion.

If one orders the counterions after the corresponding adhesion between XG and Mnt, one obtains $K^+ > Na^+ > Li^+ > Ca^{2+}$. Interestingly, this order is equivalent to the empirical Hofmeister series among cations.²⁷ Since XG is strongly amphiphilic,²⁸ it is tempting to explain the adhesion in terms of the ability of different ions to strengthen or weaken hydrophobic interactions,²⁹ similar to the salting out of proteins from aqueous solution.²⁹

However, from the ion distributions shown in Figure 4, it is clear that even if the heights and widths of the peaks are varying, virtually all ion density is located close to the interface, with only a negligible amount of ions present in the solution.

At this point it may be important to address the fact that the ion distribution resulting from the present work apparently stands in contrast to what have been observed previously using atomistic modeling. Earlier studies observe a significant ion density also in the interlayer region.^{10,11,15} However, in those studies the water content was much lower than here, leading to a considerably smaller interlayer distance. In fact, the definition of the surface region used here (0 to 8 Å, see further down) is large enough to cover the whole interlayer region in those earlier studies. So, in that respect, there is really no contradiction. Greenwell et al.^{15,30} also notes that Li^+ ions in their simulations have a tendency to penetrate into the clay octahedral layer, which was not observed here. This is likely an effect of using different potential parameters for both clay and ions.

The fact that the ions are strongly associated with the Mnt surface suggests that it is not the solution properties that control

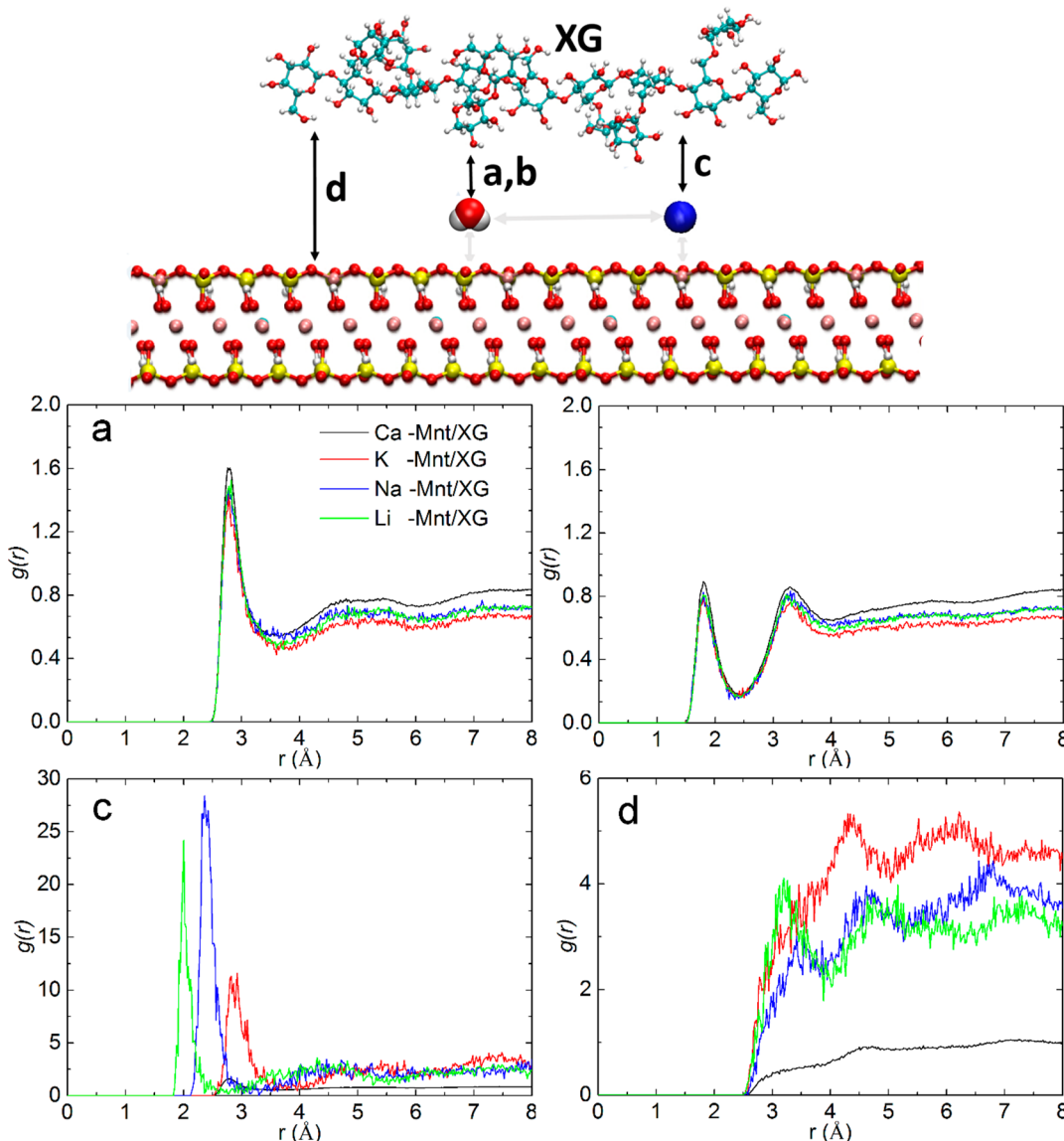


Figure 6. Top: A schematic picture of the interfacial structure, where a–d are indicating between which pairs the $g(r)$ was calculated: (a) and (b) between XG hydroxyl oxygen and water oxygen (a) or hydrogen (b); (c) between XG hydroxyl oxygen and counterions; (d) between XG hydroxyl oxygen and clay tetrahedral oxygen.

the differences in adhesion. Instead, the differences are more related to interfacial properties. To gain a more detailed understanding, the following section is devoted to the molecular structure at the interface.

Radial Distribution Functions. The complex interfacial structure was investigated using time averaged radial distribution functions (RDFs), denoted $g(r)$, calculated between different components. A schematic picture drawn on top of both Figure 5 and Figure 6 indicates the pairs for which $g(r)$ was calculated.

First, looking at the correlation between counterions and clay, one finds the largest peak to occur in the Ca-Mnt system (Figure 5b). At the same time, correlations between Ca^{2+} and XG are small compared to the other ions (Figure 6c), indicating only weak interaction. This can be interpreted as a situation where the strong electrostatic interaction between the negatively charged clays and the divalent Ca^{2+} attracts a great number of Ca^{2+} ions to the surface, and at the same time the weak interaction between XG and Ca^{2+} dispels the XG from the interface. Looking at potassium, K^+ shows more or less equal pair correlations with

both clay and XG, indicating similar interaction strength, which may help in mediating the interaction between the XG and the clay. In this picture, Na^+ would be somewhat less effective than K^+ on mediating XG/Mnt interactions, which was indeed observed in the previous section.

Looking at the $g(r)$ between XG and clay (Figure 6d), K-Mnt gives the most pronounced peak, followed by Na-Mnt and Li-Mnt, and finally, Ca-Mnt having the smallest one. However, this is merely a reflection that XG is more tightly bound to the interface in the former cases, as was concluded from Figure 4.

Looking at XG/water correlations, there are only minor differences between systems with different cations (Figure 6a,b). Nevertheless, the height of the first peak in the $g(r)$ follows the order $\text{Ca}^{2+} > \text{Li}^+ > \text{Na}^+ > \text{K}^+$, a fact that likely is due to that the XG is more tightly bound to the clay in the latter cases, thereby being less hydrated than in the former cases.

When the XG polymer adsorbs to the surface, other molecules have to be displaced to make room for it. Returning to the right panel of Figure 4, one possible explanation could be that a broad

ion distribution means that that ion species is more easily displaced than the ones with more localized distributions. If adsorption of XG onto the surface would require the displacement of ions already present there, this process would be promoted in the case of K^+ , and hardest in the case of Ca^{2+} . However, when looking at the ion distributions both before and after the XG has been detached (see Figure S5 in Supporting Information), it is evident that the differences in the distributions are small, meaning that the counterions are basically immobilized at the clay surface. However, it is still possible that the differences between the systems can be traced to the displacement of water molecules, as proposed before.

The correlation between counterions and water shown in Figure 5a reflects the order of the hydration of cations, which is $Ca^{2+} > Li^+ > Na^+ > K^+$. Experimentally, the difference in hydration free energy between K^+ and Ca^{2+} is very large, close to 290 kcal mol⁻¹.²⁹ The stronger hydration of Ca^{2+} and Li^+ leads to more coordinated water molecules both for themselves (Figure 5a), and, interestingly, also for the corresponding saturated clays (Figure 5c,d).

Altogether, the interpretation of Figures 4–6 is that the differences in calculated W_A from Figure 3 is due to competing interactions between ions (which are immobilized at the Mnt surface), water and XG. The RDFs are enlightening but can be misleading close to an interface, since the surroundings are not isotropic. The RDFs will depend on the distance from the surface, in a nontrivial way. Therefore, in the present case, one-dimensional density distributions can be more instructive, specifically for the purpose of comparing the two cases where the XG is either adsorbed to the surface, or completely detached (Figure 7). The density distributions also allow us to investigate

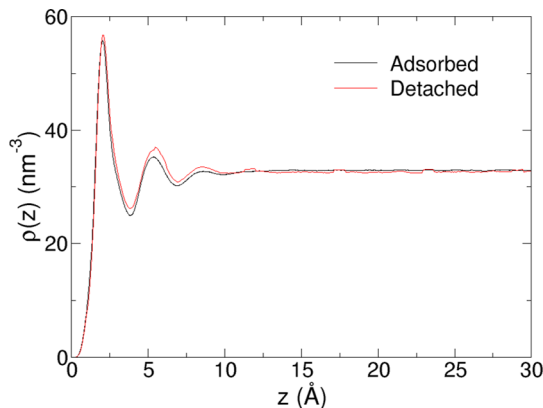


Figure 7. Water number density as a function of distance from the clay surface before (black) and after (red) pulling off the XG for the K-Mnt/XG system.

the role of water more closely, by estimating the free energy difference between bulk water and interfacial water, as will be described below.

Free Energy of Interfacial Water. Water is inevitably present at the interface, interacting with all components and influencing molecular adhesion. Figure 7 shows the water density, as a function of distance from the Mnt surface (z) before and after the XG has been pulled off for the K-Mnt/XG system. As expected, the amount of water present close to the clay surface is larger when the XG is detached, that is, water replaces XG at the interface. This also means that the ions, which are less mobilized at the surface, become more hydrated as the XG is detached.

Therefore, analogous to what has been proposed before,^{14,15} the large difference in hydration free energy between the cations is likely to be responsible for the differences in molecular adhesion observed in Figure 3. However, when the RDFs between ions and water for the case of XG fully detached are compared with RDFs with XG adsorbed to the surface (see Figures 5a and S6 in SI), no visible difference was detected. Nevertheless, even if the first hydration shells of the ions are unaffected by the presence of XG, the counterions also have long-range effects on interfacial water. This was noted above in Figure 5c, and this leads to significant differences in how strongly the water is bound to the surface. The number density presented in Figure 7 reflects the probability of finding a water molecule at a certain distance from the surface, and is thus related to the chemical potential of water. A simple step toward quantification of thermodynamic parameters is to convert the density profile, $\rho(z)$, into a potential of mean force, or work function, through

$$W(z) = -k_B T \ln \rho(z) + \text{const} \quad (1)$$

where the constant determines the zero level of the work function. This work function as a function of z is displayed in Figure 8 for the four different systems, for the case when there is

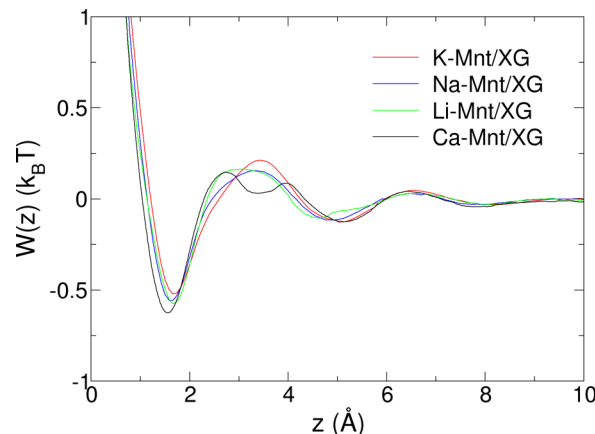


Figure 8. Potential of mean force of individual water molecules, as a function of distance from the clay surface.

no XG present at the surface. It shows small, but significant, differences between the systems. Ca-Mnt gives the deepest minimum and K-Mnt the shallowest, indicating that the water molecules have a preference for Ca-Mnt compared to K-Mnt. Na-Mnt and Li-Mnt end up in between these two. To get a measure of the relative affinity between water and Mnt in the different systems, one can calculate a difference in chemical potential, $\Delta\mu_\omega$, defined as the free energy difference between a water molecule in the surface region and one residing in an equally large volume in the bulk. A positive $\Delta\mu_\omega$ therefore indicates that water prefers to be in the bulk rather than at the interface. The difference in chemical potential is obtained by integrating $W(z)$ over z (see, e.g., Kapla et al.³¹):

$$\Delta\mu_\omega = k_B T \ln \left(\frac{1}{z_C} \int_0^{z_C} \exp(-W(z)/k_B T) dz \right) \quad (2)$$

Here z_C is an arbitrary cutoff that separates the surface region from the bulk. In the present case it was chosen to 8 Å, which is where $W(z)$ in Figure 8 flattens out. The result from eq 2 is presented in Table 2. There are significant differences between systems with different ions. First of all, it is interesting to note

Table 2. Free Energy of Interfacial Water

system	$\Delta\mu_{\omega}^a$	n_w^b	ΔG_w^{totc}	W_A^d
K-Mnt	0.036	140	5.0	26.9
Na-Mnt	0.024	170	4.1	17.5
Li-Mnt	0.024	150	3.6	15.3
Ca-Mnt	0.012	140	1.7	4.9

^aChemical potential of water, which is the free energy cost of bringing one water molecule from bulk to the interface in kcal mol⁻¹. ^bNumber of water molecules that replace XG when it is detached from the Mnt surface. ^cTotal free energy cost of expelling water molecules from the interface as XG is detached ($n_w \times \Delta\mu_{\omega}$) in kcal mol⁻¹. ^dWork of adhesion, which is the total free energy cost of detaching XG from the Mnt surface, calculated from Figure 3, for reference (in kcal mol⁻¹).

that $\Delta\mu_{\omega}$ is always positive, meaning that the water has a negative affinity for the Mnt/ion surface. It means that, from a thermodynamic point of view, despite an abundance of charged and polar moieties, water molecules prefer the bulk to the Mnt/ion surface, possibly due to favorable gain in entropy.

The calculated value for $\Delta\mu_{\omega}$ for Ca-Mnt is only half that of Na-Mnt and Li-Mnt, and one-third that of K-Mnt, clearly indicating that it is least favorable for water to be at the surface in K-Mnt, followed by Na-Mnt and Li-Mnt, and most favorable in Ca-Mnt, in accordance with the previous results for molecular adhesion of XG. Although the difference in chemical potential is very small, the detachment of a macromolecule means that a large number of water molecules must take its place at the surface. The total free energy change may thus be sufficient to make a difference. From the density profiles (such as in Figure 7), one can calculate the number of water molecules that are replacing XG at the surface upon detachment by integrating the difference between the two curves over the surface region (from 0 to 8 Å). In this case, it is found that XG is replaced by between 140 and 170 water molecules. This brings the total free energy difference up to between 1.7 kcal mol⁻¹ for Ca-Mnt and 5.0 kcal mol⁻¹ for K-Mnt. When these numbers are compared to W_A (included in Table 2 for reference), it is concluded that the free energy of replacing XG with water molecules at the surface amounts to a significant contribution to the total work of adhesion. It contributes 19% to W_A in the case of K-Mnt, 23% for Na-Mnt, 24% for Li-Mnt, and as much as 35% in the case of Ca-Mnt.

The present results reflect the different hydration energy of ions, and the consequences for the work of adhesion. In the case of K⁺, which has relatively high hydration energy, water becomes more loosely bound to the surface and is therefore more easily expelled from the interface than in the case of the other ions. This effect thus gives a positive contribution to the work of adhesion, which is largest in the case of K-Mnt, followed by Na-Mnt and Li-Mnt, and finally Ca-Mnt.

The statistical errors associated with the analysis are small due to the long simulation times. There is another source of error, which is the somewhat arbitrary choice of the cutoff z_C . Changing z_C by 1 Å, in either direction, changes $\Delta\mu_{\omega}$ by close to 20%. It is also likely that the exact proportion of $\Delta\mu_{\omega}$ to the overall W_A depends on the potential parameters for the ions and the clay and, also, on the choice of water model. However, the fact that the analysis is internally consistent makes the comparison between the different systems reliable.

CONCLUSIONS

Nanocomposites made of the polysaccharide xyloglucan and Montmorillonite clay show different tensile properties at high relative humidity when different counterions are used in the colloidal state, prior to casting of the nanocomposites. The molecular adhesion between XG and Mnt in the presence of water is an important reason, and this influences both the formation process and the stress transfer between the polymer and the clay in moist environment. The hydrated clay surface is a complex system, and an intricate balance of physical interactions between clay, water, counterions and polysaccharide determine its interfacial properties.

With MD simulations the present study shows that this effect of ions partly arise from their different hydration ability. Calculated molecular adhesion is strongest in the case of K-Mnt, followed by, in decreasing order, Na-Mnt, Li-Mnt, and Ca-Mnt. One important picture that emerges from the simulations is that the ions are less mobilized at the interface, adhering strongly to the clay through electrostatic interactions, leaving the water and the polymer to compete for the remaining space. Thus, it is the relative affinity of XG and water to the Mnt/ion surface that determines the adhesion of XG in wet systems. It has been suggested that the differences in hydration free energy among cations make water molecules more or less easily displaced from the interface, which indirectly affects the adhesion of polymer to the surface.^{14,15} A direct calculation of the chemical potential of interfacial water shows that it is indeed strongly affected by the cations. In all cases, water prefers the bulk to the Mnt surface. The free energy penalty of bringing a water molecule from the bulk to the interface region as XG detaches follows a reverse order as for the hydration free energy of the cations. It is smallest in the case of Ca-Mnt, followed by Li-Mnt and Na-Mnt, and the largest penalty is found in the case of K-Mnt. This clearly contributes to the fact that the molecular adhesion between XG and K-Mnt becomes the highest.

By estimating the number of water molecules that have to enter the interfacial region when the XG is detached, it is found that this mechanism accounts for a significant part of the total work of adhesion of XG, between 19 and 35%. However, this mechanism is not the only one since it explains only a fraction of the total work of adhesion. It is apparent that other mechanisms include specific XG/ion, XG/Mnt, and XG/water interactions. From the simulations, we make the following observations: (a) Different ions interact differently with XG and clay. Radial distribution functions reveal that Ca²⁺ interacts strongly with Mnt, but weakly with XG, which works toward expelling the polymer from the surface region. K⁺ on the other hand, interacts fairly well with both clay and polymer, which helps in mediating strong interactions between the XG and the Mnt. (b) Further, different cations interact differently with the glucan backbone, possibly leading to a decreasing rigidity in the following order: K⁺ > Na⁺ > Li⁺ > Ca²⁺. A more rigid structure in this case promotes adsorption. These two observations could not be tested unambiguously in the present setup, and therefore remain interesting topics for the future.

The present study confirms that counterions play an important role for the adhesion of Xyloglucan to Mnt clay, and indicate that counterions are very important in other nanocomposite systems as well. The present work also clarifies the mechanisms by which cations influence polymer adsorption and interfacial adhesion in polymer/clay systems. It highlights the general importance of the adsorbed polymer conformation for interfacial adhesion in moist

environment. The insights are helpful for materials design of new nanocomposite materials, where the physical and chemical properties of the material strongly depend on interface characteristics. For instance, Mnt/XG nanocomposites can be processable in water and yet show good properties in moist conditions, due to the favorable interface structure.

■ ASSOCIATED CONTENT

S Supporting Information

Additional computational details, distance between XG and Mnt as a function of simulation time, root-mean-square deviation of XG structure, hydrogen bonding between XG and water, XG radius of gyration, principal component analysis, and ion distributions and RDFs after XG is detached. This material is available free of charge via the Internet at <http://pubs.acs.org>.

■ AUTHOR INFORMATION

Corresponding Authors

*E-mail: jacke@kth.se.

*E-mail: agren@theochem.kth.se.

Notes

The authors declare no competing financial interest.

■ ACKNOWLEDGMENTS

Lars Wågberg is gratefully acknowledged for helpful insights concerning specific ion effects. Computational resources are supported by a grant from the Swedish National Infrastructure for Computing (SNIC) through the Projects “Modeling of molecular interaction between nanoparticles and polymeric molecules” (SNIC 025/12-38) and “Molecular Dynamics simulations of the interactions of organic polymers and inorganic clays” (SNIC 001/12-203). Computational support from PDC Centre for High Performance Computing (PDC-HPC) is acknowledged. Funding from SSF FireFoam (J.W. and J.K.), SSF ICA 10-0086 (M.B.-W.) and VR 2013-4058 (L.B.) is gratefully acknowledged.

■ REFERENCES

- (1) Garcia, H.; Ferreira, R.; Martins, C.; Sousa, A. F.; Freire, C. S. R.; Silvestre, A. J. D.; Kunz, W.; Rebelo, L. P. N.; Silva Pereira, C. *Biomacromolecules* **2014**, *15*, 1806–1813.
- (2) Bosmans, T. J.; Stépán, A. M.; Toriz, G.; Rennekar, S.; Karabulut, E.; Wågberg, L.; Gatenholm, P. *Biomacromolecules* **2014**, *15*, 924–930.
- (3) Bai, H.; Huang, C.; Xiu, H.; Zhang, Q.; Deng, H.; Wang, K.; Chen, F.; Fu, Q. *Biomacromolecules* **2014**, *15*, 1507–1514.
- (4) Yao, H. B.; Tan, Z. H.; Fang, H. Y.; Yu, S. H. *Angew. Chem., Int. Ed.* **2010**, *49*, 10127–10131.
- (5) Kochumalayil, J. J.; Bergensträhle-Wohlert, M.; Utsel, S.; Wågberg, L.; Zhou, Q.; Berglund, L. A. *Biomacromolecules* **2013**, *14*, 84–91.
- (6) Kochumalayil, J. J.; Morimune, S.; Nishino, T.; Ikkala, O.; Walther, A.; Berglund, L. A. *Biomacromolecules* **2013**, *14*, 3842–3849.
- (7) Heinz, H.; Vaia, R. A.; Krishnamoorti, R.; Farmer, B. L. *Chem. Mater.* **2007**, *19*, 59–68.
- (8) Suter, J. L.; Anderson, R. L.; Christopher Greenwell, H.; Coveney, P. V. *J. Mater. Chem.* **2009**, *19*, 2482–2493.
- (9) Wang, Y.; Wohlert, J.; Berglund, L. A.; Tu, Y.; Ågren, H. *J. Mater. Chem. A* **2014**, *2*, 9541–9547.
- (10) Boek, E. S.; Coveney, P. V.; Skipper, N. T. *J. Am. Chem. Soc.* **1995**, *117*, 12608–12617.
- (11) Tao, L.; Tian, X. F.; Yu, Z.; Tao, G. *Chin. Phys. B* **2010**, *19*, 109101.
- (12) Segad, M.; Jönsson, B.; Åkesson, T.; Cabane, B. *Langmuir* **2010**, *26*, 5782–5790.
- (13) Norrish, K. *Nature* **1954**, *173*, 256–257.
- (14) Bains, A. S.; Boek, E. S.; Coveney, P. V.; Williams, S. J.; Akbar, M. *V. Mol. Simul.* **2001**, *26*, 101–145.
- (15) Greenwell, H. C.; Bowden, A. A.; Chen, B.; Boulet, P.; Evans, J. R. G.; Coveney, P. V.; Whiting, A. *J. Mater. Chem.* **2006**, *16*, 1082–1094.
- (16) Cygan, R. T.; Liang, J. J.; Kalinichev, A. G. *J. Phys. Chem. B* **2004**, *108*, 1255–1266.
- (17) Kirschner, K. N.; Yongye, A. B.; Tschaumpel, S. M.; González-Outeiriño, J.; Daniels, C. R.; Foley, B. L.; Woods, R. J. *J. Comput. Chem.* **2008**, *29*, 622–655.
- (18) Berendsen, H. J. C.; Postma, J. P. M.; van Gunsteren, W. F.; Hermans, J. *Interaction Models for Water in Relation to Protein Hydration*; Springer: Netherlands, 1981; Vol. 14.
- (19) Smith, D. E.; Dang, L. X. *J. Chem. Phys.* **1994**, *100*, 3757–3766.
- (20) Koneshan, S.; Rasaiah, J. C.; Lynden-Bell, R. M.; Lee, S. H. *J. Phys. Chem. B* **1998**, *102*, 4193–4204.
- (21) van der Spoel, D.; Lindahl, E.; Hess, B.; van Buuren, A. R.; Apol, E.; Meulenhoff, P. J.; Tielemans, D. P.; Sijbers, A. L. T. M.; Feenstra, K. A.; van Drunen, R.; Berendsen, H. J. C. *Gromacs User Manual*, version 4.5.4; Gromacs: Stockholm, Sweden, 2010.
- (22) Berendsen, H. J. C.; van der Spoel, D.; van Drunen, R. *Comput. Phys. Commun.* **1995**, *91*, 43–56.
- (23) Lindahl, E.; Hess, B.; van der Spoel, D. *J. Mol. Model.* **2001**, *7*, 306–317.
- (24) van der Spoel, D.; Lindahl, E.; Hess, B.; Groenhof, G.; Mark, A. E.; Berendsen, H. J. C. *J. Comput. Chem.* **2005**, *26*, 1701–1719.
- (25) Hess, B.; Kutzner, C.; van der Spoel, D.; Lindahl, E. *J. Chem. Theory Comput.* **2008**, *4*, 435–447.
- (26) Humphrey, W.; Dalke, A.; Schulten, K. *J. Mol. Graph.* **1996**, *14*, 33–38.
- (27) Hofmeister, F. *Arch. Exp. Pathol. Pharmacol.* **1888**, *24*, 247–260.
- (28) Mishra, A.; Malhotra, A. V. *J. Mater. Chem.* **2009**, *19*, 8528–8536.
- (29) Marcus, Y. *Chem. Rev.* **2009**, *109*, 1346–1370.
- (30) Chen, B.; Evans, J. R.; Greenwell, H. C.; Boulet, P.; Coveney, P. V.; Bowden, A. A.; Whiting, A. *Chem. Soc. Rev.* **2008**, *37*, 568–594.
- (31) Kapla, J.; Wohlert, J.; Stevensson, B.; Engström, O.; Widmalm, G.; Maliniak, A. *J. Phys. Chem. B* **2013**, *117*, 6667–6673.